Research Square

Preprints are preliminary reports that have not undergone peer review.
They should not be considered conclusive, used to inform clinical practice,
or referenced by the media as validated information.

Crop Type Mapping in Smallholder and Complex Agricultural Landscapes Using Multi-Temporal Sentinel-2 Imagery on the Google Earth Engine Platform

Masoumeh Aghababaei

ma.aghababaeei@stu.sku.ac.ir

Shahrekord University

Elham KianiSalmi

Lorestan University

Ataollah Ebrahimi

Shahrekord University

Research Article

Keywords: Multi-temporal images, Crop type mapping, Google Earth Engine, Smallholder agriculture, Transformed Divergence

Posted Date: August 12th, 2026

DOI: https://doi.org/10.21203/rs.3.rs-10609969/v1

License: This work is licensed under a Creative Commons Attribution 4.0 International License.
Read Full License

Additional Declarations: No competing interests reported.

Abstract

This study addresses the challenge of accurate crop type mapping in heterogeneous smallholder agricultural landscapes where orchards and annual crops are intermingled, resulting in significant spectral overlap and seasonal asynchrony. We develop a hybrid framework integrating multi-temporal Sentinel-2 imagery (2020–2022), topographic covariates (DEM, slope, aspect), and phenological analysis within the Google Earth Engine (GEE) platform. The study area, Saman County (Chaharmahal-Va Bakhtiari Province, Iran)—a major almond and peach production hub—was classified into nine crop classes. NDVI time-series analysis combined with the Transformed Divergence (TD) index identified May-September as the optimal temporal window for maximum class separability. Following masking of residential areas and riverbeds, and incorporating topographic layers, a Random Forest (RF) algorithm trained on 70% of 1,500 field-sampled points achieved 95% overall accuracy and strong agreement with agricultural statistics ($R^2 = 0.96$, $p < 0.01$). This framework demonstrates that integrating phenology-guided temporal composites, physiographic variables, and machine learning within GEE provides a scalable and efficient solution for accurate crop mapping in complex smallholder systems, supporting sustainable land management and irrigation optimization.

Introduction

Accurate and timely crop type mapping underpins effective agricultural monitoring, food security planning, and sustainable resource management (Jin et al., 2019; Huang et al., 2026). These maps facilitate yield estimation, cropping pattern optimization, pest and disease surveillance, and policy formulation (Narimani et al., 2026). Remote sensing has emerged as the most efficient approach for large-scale crop mapping, yet significant challenges persist in heterogeneous agricultural landscapes. In the patchwork agricultural landscapes of Iran's Saman County the nation's foremost hub for almond and peach production orchards and annual crop fields are so intimately intermingled that their spectral signatures bleed into one another, confounding conventional satellite-based classification methods. Mapping crop types in smallholder-dominated regions faces three primary challenges: irregular field geometries, mixed cropping systems, and spectral similarities between cultivated and natural vegetation (Heiss et al., 2025). These factors render single-date imagery inadequate, as crop spectral reflectance varies considerably across phenological stages (Ashourloo et al., 2022). Multi-temporal imagery acquired during critical growth stages can capture these phenological variations and improve classification accuracy. However, determining the optimal acquisition timing remains challenging (Rehman et al., 2025). Processing all available imagery is computationally intensive and costly, while empirical timing selection lacks systematic validation (Chang et al., 2025). A phenology-based approach for intelligent selection of multi-temporal data offers a more efficient solution for spectral differentiation of agricultural crops (Aghababaei et al., 2024).

Previous studies have demonstrated the value of strategic temporal sampling. Low et al. (2015) demonstrated that only five key RapidEye images acquired at shooting, heading, and grain-filling stages achieved equivalent classification accuracy for wheat, canola, and barley compared to using all available

imagery. Similarly, Hill et al. (2018) reported that using eight Sentinel-2 images throughout the growing season increased apple and pear orchard classification accuracy from 57% (single image) to 89%, with only three strategically selected images (post-flowering, fruiting, autumn senescence) achieving 86% accuracy substantially reducing data volume and processing costs.

Gitas et al. (2019) achieved only 60% accuracy differentiating olive and fig trees using spring and summer imagery, but inclusion of an early autumn image capturing fig foliage yellowing against still-green olive canopies, combined with NDVI, increased accuracy to 92%. Kussul et al. (2017) demonstrated that Sentinel-2 time-series analysis could effectively separate apple orchards from wheat and rice using only mid-growth stage imagery, when apple trees exhibit maximum canopy development while cereals transition to heading and grain-filling phases. These findings collectively indicate that while time-series imagery is necessary, understanding crop phenology and precise image timing selection are critical for classification success.

Google Earth Engine (GEE) has become a widely adopted platform for large-scale remote sensing analyses, including land use/land cover mapping (Machireddy, 2023), ecological unit monitoring (Aghababaei et al., 2025), and forest dynamics assessment (Zhang et al., 2025). While remote sensing has proven effective for crop mapping, most studies have focused on regions with homogeneous spatial patterns and farm structures (Peng et al., 2023; Zhu et al., 2023). In contrast, our study area features a small-scale, heterogeneous agricultural landscape where orchards coexist with rice, wheat, and barley plots, exhibiting seasonal asynchrony. Under such conditions, significant spectral overlap among crop types limits the utility of medium-spatial-resolution sensors, whose imagery often misses critical phenological windows for discrimination (Eisfelder et al., 2024). Identifying sensitive growth periods and deriving discriminative phenological indices from high-temporal-resolution Sentinel-2 data (10–20 m, 5-day revisit) is therefore essential (Chabalala et al., 2023; Narimani et al., 2026). Additionally, topographic variables (DEM, slope, aspect) influence phenological timing and spectral responses and must be considered (Benoumeldjadj et al., 2025).

The choice of classification algorithm critically influences mapping accuracy. Machine learning methods applied to time-series and spectral data have proven highly effective (Pena et al., 2017; Liakos et al., 2018). Among these, Random Forest (RF) excels at handling complex nonlinear relationships, performing inherent feature selection, and resisting noise and outliers (Wang et al., 2021; Aghababaei et al., 2022).

This study aims to improve crop type separability in smallholder and intercropped systems where conventional classification methods suffer from spectral confusion and estimation bias. We pursue two primary objectives: (1) conduct a systematic analysis of phenological differences among nine crop classes (including fruit trees and annual species) using multi-temporal Sentinel-2 data to identify an optimal temporal composite maximizing spectral divergence; and (2) develop a hybrid classification framework integrating multi-temporal Sentinel-2 imagery with topographic covariates (DEM, slope, aspect) implemented on GEE using the Random Forest algorithm. The resulting crop type map is

expected to provide an accurate spatial representation of orchards and farms, offering local planners and experts quantitative support for continuous monitoring, irrigation optimization, and sustainable land management.

Materials and Methods

Study Area

Saman County is located approximately 22 km northeast of Shahrekord, the capital of Chaharmahal-Va Bakhtiari Province, Iran, along the banks of the Zayandeh-Rood River (centered at approximately 32.55°N, 50.92°E; elevation range: 1,800-2,400 m a.s.l.) (Fig. 1). As the leading producer of almonds and peaches in Iran (Khalili-Moghadam & Saeidi, 2023), this county represents a strategic horticultural hub critical to the regional agricultural economy and food security. The landscape is characterized by smallholder cultivation where various orchard types (almond, peach, walnut, cherry, grape, apricot, apple) are interspersed with scattered annual crop fields (rice, wheat, barley). This intermingling of horticultural and field crops, combined with small field sizes and irregular boundaries, substantially complicates accurate crop type mapping and necessitates improved methodologies.

Figure 1. Location of the study area: (a) Chaharmahal-Va-Bakhtiari province boundary; (b) study area boundary (Saman district). A set of sampling points was collected from agricultural areas. The sampling points were subsequently divided into two groups: 70% for training the crop-type classification model and 30% for testing and validation mapping.

Field Data Collection

The primary objective of this study was to generate an accurate crop-type map integrating field observations with remote sensing data. Based on annual agricultural yearbook reports and consultations with local agricultural extension experts, nine agricultural classes were identified as the primary classification targets (Fig. 2): almond, peach, walnut, cherry, grape, apricot, apple, rice, and wheat-barley (combined due to spectral similarity and similar phenological cycles).

Ground truth data were collected using a dual-frequency GPS with centimeter-level accuracy (Trimble GeoXH, ± 10 cm horizontal accuracy). Field campaigns were conducted during the peak growing season (June-July 2022) to maximize visual distinguishability among crop types. A total of 1,500 valid field survey points were recorded (Fig. 1), stratified by crop type, elevation, and slope position to ensure representation of the region's topographic diversity. The sample size was determined based on the Minimum Acceptable Sample Size (MASS) formula for crop classification studies ($n \geq 10–30$ per class per 100 ha of cultivated area). These points were partitioned into training (70%; n = 1,050) and independent validation (30%; n = 450) subsets using stratified random sampling to maintain class proportion. Following final map generation, classification accuracy was quantitatively assessed using error matrix analysis (Aghababaei et al., 2021a).

Figure 2. Percentage of cultivated area for selected agricultural crop types, based on the Agricultural Yearbook.

Methodology

Residential Area Masking

One significant challenge in the study area is the uncontrolled expansion of villa settlements and conversion of agricultural lands to residential/recreational uses, which introduces mixed-pixel errors in classification. To address this, we computed NDVI for images acquired during the active growing season (May, June, July) and generated a false-color composite (RGB = NDVI_May, NDVI_June, NDVI_July). This composite effectively discriminated vegetated from non-vegetated surfaces. Using threshold segmentation (NDVI < 0.3 for residential areas, validated against high-resolution Google Earth imagery), we extracted a binary mask layer representing residential and built-up areas, which was then applied to exclude these pixels from all subsequent analyses (Fig. 3).

Figure 3. Separation of residential areas and generation of the mask layer. (a) False-color composite of NDVI; (b) Mask layer produced by excluding residential areas.

Optimal Temporal Window Selection (using TD)

Single-date imagery is insufficient for accurate crop type mapping in this region due to distinct phenological behaviors of orchards versus annual crops. To characterize these dynamics, NDVI time series were generated within GEE for 2020–2022 using all available Sentinel-2 imagery with < 5% cloud cover. Three years were selected to minimize the influence of inter-annual climatic variations and ensure the consistency of phenological patterns. For each reference point, NDVI profiles were extracted and plotted across the growing season to visualize the spectral-temporal behavior of each crop class.

To quantitatively identify the optimal temporal window, the Transformed Divergence (TD) statistical index was employed as a criterion to select the optimal time intervals that provide maximum separability among crop types. The TD index measures class separability as:

$$TD = 2000[1 - \exp(-D/8)]$$

where D is the Divergence measure calculated from the mean vectors and covariance matrices of each class pair. Following the standard threshold established by Swain and Davis (1978) and subsequently applied by Mishra and Susaki (2014), TD values > 1.5 indicate good to excellent separability, while values < 1.0 suggest poor class discrimination.

For each of the three study years, monthly NDVI composites were generated, and TD values were calculated between all class pairs. The average TD value for each month was computed to identify

periods with maximum overall class separability. Months with TD values consistently exceeding 1.5 across all three years were selected for inclusion in the optimal temporal composite.

Based on this quantitative analysis, combined with visual interpretation of the NDVI time-series profiles, the months of May, June, July, August, and September were identified as the optimal temporal window for crop type classification (Table 1; Fig. 6). During this period, the spectral differences among crops are maximized due to distinct phenological stages, including canopy development, flowering, fruit setting, and senescence. Months outside this window (October–February) exhibited TD values well below 1.5, indicating poor class separability and were consequently excluded from the classification dataset.

Table 1
Transformed Divergence (TD) values obtained for monthly composites across the three study years (2020–2022).

2020		**2021**		**2022**	
Month	TD	Month	TD	Month	TD
July	1.83	**July**	1.74	**July**	1.76
June	1.78	**August**	1.65	**June**	1.68
August	1.74	**June**	1.59	**August**	1.62
September	1.68	**September**	1.50	**May**	1.49
May	1.63	May	1.49	September	1.47
October	1.45	October	1.22	April	1.25
April	0.92	April	1.18	October	1.18
November	0.87	November	0.84	November	0.89
March	0.69	March	0.63	March	0.72
December	0.62	December	0.59	December	0.62
January	0.51	February	0.52	January	0.51
February	0.48	January	0.46	February	0.48

Final Input Data Preparation

Topographic variables (DEM, slope, aspect) were derived from the ASTER GDEM v3 (30 m resolution) and resampled to 10 m using bilinear interpolation to account for environmental factors influencing crop distribution. Sentinel-2 Level-2A surface reflectance images were acquired for 2020–2022 with ≤ 5% cloud cover. Bands at 10 m spatial resolution (B2, B3, B4, B8) and 20 m resolution (B5, B6, B7, B8a, B11, B12) were included, with 20 m bands resampled to 10 m using the bicubic method. All spectral bands, topographic layers, and monthly composites were combined into a multi-layer input stack for

classification. Following evaluation of multiple algorithms (Support Vector Machine, Classification and Regression Trees, RF), the Random Forest algorithm was selected for final classification due to its superior performance and robustness. The RF parameters were: n_trees = 80, m_try = √p (where p = number of features), minimum leaf size = 1, and out-of-bag error estimation. Classification was implemented within the GEE JavaScript API using the ee.Classifier.smileRandomForest function.

Comparison with Agricultural Statistics

Estimated cultivated areas for each crop class derived from the classification map were compared against official statistics from the Agricultural Statistical Yearbook (2022 crop year). Simple linear regression (OLS) and coefficient of determination (R^2) were used to quantify agreement, with scatter plots generated for visual assessment. A 1:1 reference line was overlaid to evaluate systematic bias.

Figure 4. Methodological workflow for crop type mapping: (1) Sentinel-2 image acquisition and preprocessing; (2) NDVI time-series analysis and optimal temporal window selection via TD; (3) Residential area masking using NDVI false-color composites; (4) Incorporation of topographic layers; (5) RF classification on GEE; (6) Accuracy assessment using independent validation points; (7) Comparison with agricultural statistics.

Results

Optimal Temporal Window Selection

NDVI time-series profiles for nine crop classes over 2020–2022 revealed three distinct phenological functional groups (Fig. 5). Group 1 (early-summer peak crops: cherry, walnut, wheat-barley, apricot) reached maximum spectral coefficients between May-July, declining from August onward as harvest progressed. Group 2 (late-season peak crops: rice, peach, almond, apple) exhibited low NDVI in May-June, then accelerated growth from late July, peaking in August-September. Group 3 (stable phenology: grape) showed gradual linear increases across all months, maintaining intermediate NDVI values throughout.

TD analysis (Table 1) identified June-August as having TD values consistently > 1.5 across all three years (mean TD = 1.71 ± 0.09), confirming maximum class separability. May and September showed TD values near 1.5 (mean = 1.54 ± 0.08 and 1.55 ± 0.11, respectively) and were included to enhance classification accuracy. Months outside this window (October-February) exhibited TD < 1.5 (range: 0.46–1.45), indicating poor class separability (Mishra & Susaki, 2014).

Based on these results, the optimal temporal composite included Sentinel-2 imagery from May, June, July, August, and September (Fig. 6), with specific acquisition dates selected based on cloud cover (< 5%) and image quality.

Figure 5. Spectral-temporal curves of the NDVI for 9 agricultural crop types in the years 2020–2022.

Table 1. Transformed Divergence (TD) values obtained for monthly composites across the three study years (2020–2022).

Figure 6. Best-performing Sentinel-2 temporal composites for crop type mapping.

Crop Type Classification and Accuracy Assessment

Applying the RF algorithm to the optimal temporal composite and topographic covariates produced a crop type classification map (Fig. 7). Spatial distribution shows almond as dominant (10,960 ha, 65.4%), followed by peach (2,482 ha, 14.8%), walnut (1,849 ha, 11.0%), and smaller areas of cherry (419 ha), grape (395 ha), apricot (281 ha), and apple (132 ha). Annual crops (barley-wheat: 354 ha; rice: 46 ha) occupied only 2.4% of cultivated area, typically in small scattered parcels.

Accuracy assessment based on the independent validation subset (n = 450) yielded overall accuracy = 95% (Kappa = 0.94 ± 0.02). Producer's accuracy (PA) and User's accuracy (UA) varied by class (Fig. 8; Table 2). Barley-wheat achieved the highest PA (98.6%), while apricot showed the lowest PA (90.1%). Almond demonstrated the highest UA (98.3%), and walnut the lowest (85.6%). The main confusion sources were spectral overlap between walnut and apple (commission error: 12.5% for apple, 14.2% for walnut) and peach-apricot confusion in early stages (omission error: 8.5% for peach).

Figure 7. Crop type classification mapping.

Quantitative accuracy assessment, derived from the error matrix (Fig. 8), demonstrated high classification performance, with an overall accuracy of 95% and a Kappa coefficient of 0.94. Per-class producer’s accuracy (PA) and user’s accuracy (UA) indicated robust model performance across most crop types. Barley-wheat achieved the highest PA (98.6%), whereas apricot exhibited the lowest, though still within an acceptable range (90.1%). Conversely, UA was highest for almond (98.3%) and lowest for walnut (85.6%).

For several classes, notable discrepancies between PA and UA were observed, reflecting trade-offs between omission and commission errors. Specifically, the differences between PA and UA (i.e., PA minus UA) were 5.2 percentage points for apple and 5.7 percentage points for rice, indicating that these classes were prone to over-prediction (i.e., higher commission errors). In contrast, cherry exhibited a balanced performance, with a UA of 98.5% and a PA of 92.4%, suggesting minimal systematic bias for this class.

Figure 8. Comparison of Producer's Accuracy and User's Accuracy by Crop Type

Comparison with Agricultural Statistics

Comparison of map-derived areas with agricultural statistics (Fig. 9) showed strong agreement (R^2 = 0.964; y = 1.033x + 149.97; n = 9). The slope (1.033, 95% CI: 0.968–1.098) and intercept (149.97 ha, 95%

CI: -15.2 to 315.1) indicate a slight but non-significant overestimation bias for smaller classes. Per-class assessment (Fig. 10) revealed strongest agreement for almond (difference: +2.8%), barley-wheat (+ 1.2%), and rice (+ 3.1%), consistent with their more homogeneous spatial patterns. Larger discrepancies occurred for walnut (-8.1%), apple (-7.3%), and apricot (+ 6.8%), likely reflecting fragmentation and spectral confusion issues discussed above.

Figure 9. Scatter Plot comparing the cultivated area from statistical yearbooks and the crop type classified map.

Figure 10. Per-class scatter plots comparing map-derived cultivated areas with official agricultural statistics for each crop type.

Discussion

Effectiveness of Residential Area and River Masking

A critical preprocessing step in this study was the generation of a mask layer to exclude residential areas and the Zayandeh-Rood River corridor. This was accomplished using a false-color composite of NDVI images from May, June, and July, which effectively discriminated vegetated surfaces from non-vegetated built-up areas and water bodies.

In smallholder-dominated landscapes, agricultural fields are often fragmented and interspersed with settlements, leading to mixed pixels that reduce classification accuracy. The phenomenon of agricultural land conversion to residential and recreational uses, particularly pronounced in peri-urban areas like Saman County, not only disrupts ecological balance but also introduces spectral contamination that obscures crop signatures. Asgarian (2026) similarly emphasized that masking such features is essential for enhancing classification accuracy in mixed land-use environments. Our approach, which applied an NDVI threshold of < 0.3 to extract residential pixels, proved effective: the masking procedure reduced spectral confusion and improved per-class accuracy by an estimated 12–18% in preliminary tests. This aligns with findings from Mirzaei et al. (2020), who demonstrated that incorporating secondary data layers, including masks for non-agricultural land, can increase overall classification accuracy by 3–10%.

Furthermore, the presence of the Zayandeh-Rood River, with its seasonally fluctuating water levels, posed additional challenges. Riverbanks and riparian zones often exhibit spectral signatures similar to irrigated crops, particularly rice. By masking the river corridor and its buffer zone, we minimized this source of error. This practice is increasingly recognized as a necessary step in operational crop mapping, particularly in regions where surface water bodies intersect agricultural areas.

Phenological Characterization and Optimal Temporal Window Selection

The systematic analysis of NDVI time-series profiles across the 2020–2022 growing seasons revealed three distinct phenological functional groups among the nine crop classes, providing the foundation for selecting the optimal temporal window for classification.

Group 1 comprising cherry, walnut, wheat-barley, and apricot exhibited early-summer peaks (May–July), with NDVI values declining sharply from August onward as harvest progressed. Group 2 including rice, peach, almond, and apple displayed a contrasting pattern, with low NDVI in early summer and accelerated growth from late July, peaking in August–September. Group 3, represented solely by grape, showed a remarkably stable phenological trajectory with gradual linear increases throughout the season. These findings are consistent with recent studies demonstrating that phenology-based metrics derived from Sentinel-2 time series can effectively delineate orchard, vineyard, and tree crops. Indeed, research in Southern France showed that phenology metrics derived from Sentinel-2 time series successfully discriminated fruit trees, vineyards, and olive groves (Abubakar et al., 2023). Similarly, a study in Iran demonstrated that NDVI features alone achieved 93.65% accuracy in discriminating olive and citrus orchards, confirming the dominant discriminative role of phenological information (Benzhair et al., 2026).

The TD statistic provided quantitative confirmation of our visual interpretations. Months with TD values exceeding 1.5, specifically June, July, and August, were identified as providing acceptable to excellent class separability, consistent with the standard threshold established by Mishra and Susaki (2014). The inclusion of May and September (TD ≈ 1.5) further enhanced discrimination. Importantly, our TD-based selection achieved 95% overall accuracy using only five monthly composites, comparable to the 89–92% accuracy reported by Hill et al. (2018) using 3–8 images, while reducing data volume by approximately 60%. This finding underscores the value of strategic temporal sampling over exhaustive data collection, a principle that is particularly relevant for operational monitoring in resource-constrained settings. The approach also aligns with the work of Qi et al. (2024), who demonstrated that multi-year mapping of cropping systems in smallholder regions can be effectively accomplished using optimized Sentinel-2 time series within GEE. The temporal patterns observed here also have implications for distinguishing perennial crops from annuals. As noted by researchers working in similar contexts, the mid-to-late summer period (July–September) provides the greatest discriminating power for separating permanent tree crops from cereals. During this window, fruit trees are at maximum canopy development while cereals are senescing, resulting in distinctly different spectral responses. Our results corroborate this finding: the highest-class separability coincided with this period, when Group 1 crops were declining and Group 2 crops were reaching their peaks.

Contribution of Topographic Variables to Classification Accuracy

The integration of DEM, slope, and aspect as auxiliary inputs proved instrumental in reducing spectral overlap among classes with similar phenological signatures, particularly walnut-apple and peach-apricot. The observed spatial distribution patterns reflect species-specific ecological niches and management practices, creating a "topographic stratification" that complements spectral discrimination.

At the lowest elevations and flattest slopes, rice, as a flooded crop, was exclusively established, a pattern consistent with findings from Southeast Asian floodplains (Zhan et al., 2022) and the Mekong Basin (Liu et al., 2024). In low-to-middle elevations with gentle slopes, peaches and apricots dominated, with peaches favoring south-facing aspects for maximum solar radiation and apricots preferring eastern aspects to avoid hot westerly winds. At middle elevations with moderate slopes, walnuts, apples, and grapes formed a competitive zone, with walnuts preferentially established on northern aspects for moisture retention, while rainfed grapes occupied steeper southern slopes for enhanced sugar accumulation. At the highest elevations with steep slopes, almonds and cherries emerged as the dominant species, with drought-tolerant almonds concentrated on southern aspects and cold-tolerant cherries on northern aspects.

This topographic patterning is not merely descriptive but has practical implications for classification. By incorporating these layers, we effectively recreated the "topographic memory" of the landscape, the ecological rules governing species distribution, which reduced commission errors for walnut (from > 20% in preliminary models without topography to 14.2%) and apple (from > 18% to 12.5%). The quantitative improvement (approximately 12–15% reduction in confusion between these classes) is consistent with broader findings in the literature. Studies have shown that incorporating thermal data, slope angle, and DEM can increase overall land use classification accuracy by 3–10%. Similarly, research on agricultural area identification has demonstrated that key topographic variables of altitude, slope, and aspect are essential for accounting for terrain characteristics that influence agricultural land use. The value of topographic data in crop mapping is increasingly recognized. As noted by researchers, elevation data is essential for the proper classification of land use and land cover by remote sensing techniques (Bihatowicz et al., 2024). The aspect problem, whereby slopes facing different directions receive varying solar radiation, affecting vegetation growth and spectral response, can only be properly addressed by utilizing suitable digital elevation data in conjunction with remote sensor response. Our study confirms that the simultaneous integration of the topographic triad (DEM, slope, aspect) provides a three-dimensional framework that enables highly accurate discrimination of crop distribution and the ecological niche of each species.

Random Forest Performance and Comparison with Other Studies

The Random Forest algorithm achieved an overall accuracy of 95% with a Kappa coefficient of 0.94, demonstrating robust performance across the nine crop classes. This result compares favorably with other studies employing RF for crop classification on parcel-based crop-type classification using Sentinel-1/2 time series (Mobarakeh et al., 2025).

The per-class accuracy metrics revealed important patterns. Almond, the dominant class covering over 65% of the area, achieved the highest user's accuracy (98.3%), reflecting its extensive spatial footprint and relatively homogeneous spectral signature. Barley-wheat achieved the highest producer's accuracy (98.6%), attributable to its uniform row-cropping pattern and distinct phenological cycle. Conversely,

walnut exhibited the lowest user's accuracy (85.6%), with a commission error exceeding 14%, primarily due to spectral overlap with apple and natural dispersion at high altitudes. This confusion between walnut and apple is a known challenge in remote sensing, as both species exhibit similar canopy structure and phenological timing in certain periods (Zhou et al., 2022)

The class imbalance issue, where almond comprised > 65% of samples while rice occupied only 0.3%, likely contributed to the lower user's accuracy for minority classes. Rice achieved a producer's accuracy of 94.2% but a user's accuracy of only 88.3%, indicating that the model tended to over-predict rice. This pattern is consistent with findings from studies on imbalanced datasets in crop classification, where minority classes are often under-represented in training samples. Strategies such as cost-sensitive learning or synthetic oversampling could potentially address this limitation in future work.

The superior performance of RF in this study can be attributed to several factors: (1) its ability to handle high-dimensional data with complex nonlinear relationships; (2) inherent feature selection, which reduces overfitting; (3) robustness to noise and outliers; and (4) efficient processing of large-scale data within the GEE environment. These advantages are well-documented in the literature (Wang et al., 2021; Aghababaei et al., 2021b).

Comparison with Agricultural Statistics: Validation and Implications

The strong agreement between map-derived areas and official agricultural statistics (R^2 = 0.964; y = 1.033x + 149.97) provides independent validation of our classification approach. The slope slightly greater than 1 (1.033) and positive intercept (149.97 ha) indicate a minor tendency for the map to overestimate official statistics for smaller classes, though this bias was not statistically significant (95% CI for slope: 0.968–1.098).

The per-class scatter plots revealed interesting patterns. Almond, with its large and relatively contiguous cultivation area, showed the closest agreement between map and statistics (difference: +2.8%). Barley-wheat and rice also demonstrated strong agreement (+ 1.2% and + 3.1%, respectively), reflecting their more homogeneous spatial patterns. In contrast, walnut (− 8.1%), apple (− 7.3%), and apricot (+ 6.8%) showed larger discrepancies, consistent with their fragmented distribution and spectral confusion issues discussed above.

These discrepancies highlight the challenges of mapping small, scattered orchard plots in heterogeneous landscapes. As noted by researchers working in similar contexts, smallholder farms are characterized by small field sizes, irregular boundaries, and intercropping, all of which complicate accurate area estimation. The use of Sentinel-1/2 data fusion has been proposed as a strategy to improve crop mapping accuracy in such systems. Monthly aggregated data, in particular, has been shown to best capture crop phenology across smallholder agricultural landscapes.

The strong correlation between our map-derived areas and official statistics has practical implications. It suggests that our approach can provide reliable estimates of cultivated area for major crops, supporting applications such as yield forecasting, irrigation planning, and policy formulation. For local planners in Saman County, this framework offers a cost-effective means of monitoring cropping patterns and tracking land use changes, capabilities that are increasingly important given the pressures of urban expansion and climate variability.

Conclusions

This study demonstrates that intelligent integration of multi-temporal Sentinel-2 data, topographic covariates, and phenological knowledge provides an efficient and reliable solution for crop type mapping in complex, smallholder-dominated agricultural landscapes. Key innovations include: (1) TD-based temporal optimization identifying May-September as the optimal window, reducing data volume by ~ 60% while maintaining high accuracy; (2) topographic stratification reducing spectral confusion; and (3) GEE-based implementation enabling operational, cost-effective processing at scale. The resulting 95% overall accuracy map reveals almond as the dominant crop (65.4% of cultivated area), with peach, walnut, and smaller orchard crops comprising the remainder. Strong agreement with agricultural statistics (R^2=0.96) confirms map reliability for practical applications. For local planners, this framework provides accurate, timely maps of crop distribution for monitoring cropping patterns, optimizing irrigation, tracking land use changes, and supporting sustainable agricultural policies.

This approach is readily transferable to other regions with high crop diversity and fragmented smallholder systems. Future work should focus on: (1) integrating Sentinel-1 SAR data for cloud-obscured periods; (2) developing adaptive algorithms for real-time mapping; (3) exploring cost-sensitive learning for imbalanced classes; and (4) coupling with yield models for integrated monitoring systems. Such advances will further enhance the utility of remote sensing for agricultural management in complex landscapes worldwide.

Declarations

Conflicts of Interest

The authors declare no conflict of interest.

Funding

This work was supported by Shahrekord University and Agricultural Jihad Organization of Chaharmahal-Va Bakhtiari Province.

Author Contribution

Masoumeh Aghababaei: Software, Investigation, Resources, Conceptualization, Methodology, Data Curation, Writing - Original Draft.Elham KianiSalmi: Software, Writing. Ataollah Ebrahimi: Validation, Review & Editing.

Acknowledgement

During the preparation of this manuscript, the authors used DeepSeek-V3-0324 (DeepSeek Company) for drafting and refining the English text of the Highlights section, as well as for language polishing of specific technical descriptions. The authors have reviewed, edited, and verified all AI-generated outputs and assume full responsibility for the final content of this publication.

Data Availability Statement

Data supporting this study may be provided by the first author upon a reasonable request. The data are not publicly available due to the privacy of parts of the data.

References

1. Abubakar, M. A., Chanzy, A., Flamain, F., Pouget, G., & Courault, D. (2023). Delineation of orchard, vineyard, and olive trees based on phenology metrics derived from time series of Sentinel-2. Remote Sensing, 15(9), 2420. https://doi.org/10.3390/rs15092420
2. Aghababaei, M., Ebrahimi, A., Naghipour, A. A., Asadi, E., & Verrelst, J. (2021a). Classification of plant ecological units in heterogeneous semi-steppe rangelands: Performance assessment of four classification algorithms. Remote Sensing, 13(17), 3433. https://doi.org/10.3390/rs13173433
3. Aghababaei, M., Ebrahimi, A., Naghipour, A. A., Asadi, E., & Verrelst, J. (2021b). Vegetation types mapping using multi-temporal Landsat images in the Google Earth Engine platform. *Remote Sensing*, *13*(22), 4683. https://doi.org/10.3390/rs13224683
4. Aghababaei, M., Ebrahimi, A., Naghipour, A. A., Asadi, E., Perez-Suay, A., Morata, M., Garcia, J. L., Rivera Caicedo, J. P., & Verrelst, J. (2022). Introducing ARTMO's machine-learning classification algorithms toolbox: Application to plant-type detection in a semi-steppe Iranian landscape. *Remote Sensing*, *14*(18), 4452. https://doi.org/10.3390/rs14184452
5. Aghababaei, M., Ebrahimi, A., Naghipour, A. A., Asadi, E., & Verrelst, J. (2024). Monitoring of plant ecological units cover dynamics in a semiarid landscape from past to future using multi-layer perceptron and Markov chain model. *Remote Sensing*, *16*(9), 1612. https://doi.org/10.3390/rs16091612
6. Aghababaei, M., Ebrahimi, A., Naghipour, A. A., Asadi, E., & Verrelst, J. (2025). Enhancing plant ecological unit mapping accuracy with auxiliary data from Landsat-8 in a heterogeneous rangeland.

Remote Sensing, *17*(24), 4025. https://doi.org/10.3390/rs17244025

7. Asgarian, A. (2026). The illusion of spectral greening: Unveiling the hidden transformation of agricultural land use in an arid peri-urban landscape of central Iran. *Journal of Arid Environments*, *233*, Article 105560. https://doi.org/10.1016/j.jaridenv.2026.105560
8. Ashourloo, D., Nematollahi, H., Huete, A., Aghighi, H., Azadbakht, M., Shahrabi, H. S., & Goodarzdashti, S. (2022). A new phenology-based method for mapping wheat and barley using time-series of Sentinel-2 images. *Remote Sensing of Environment*, *280*, 113206. https://doi.org/10.1016/j.rse.2022.113206
9. Benoumeldjadj, M., Guechi, I., Lakehal, A., & Boucherab, A. (2025). Assessment of agricultural suitability through remote sensing: A Google Earth Engine and GIS-based approach for integrated urban planning. *Journal of Agrometeorology*, *27*(3), 299–306.
10. Benzhair, F., Elyoussfi, H., Baba, W. M., Azamz, R., & Belaqziz, S. (2026). Enhanced discrimination of olive and citrus orchards in semi-arid regions using Sentinel-1/2 data fusion and hybrid texture phenology features. In *2026 IEEE Mediterranean and Middle-East Geoscience and Remote Sensing Symposium (M2GARSS)* (pp. 378–382). IEEE. https://doi.org/10.1109/M2GARSS67833.2026.11581923
11. Bihatowicz, J., Rogula-Kozłowska, W., Gromek, P., & Bihatowicz, J. S. (2024). What is the actual composition of specific land cover? An evaluation of the accuracy at a national scale – Remote sensing in comparison to topographic land cover. *Remote Sensing Applications: Society and Environment*, *36*, Article 101319. https://doi.org/10.1016/j.rsase.2024.101319
12. Chabalala, Y., Adam, E., & Kganyago, M. (2023). Mapping fruit tree dynamics using phenological metrics from optimal Sentinel-2 data and Deep Neural Network. *CABI Agriculture and Bioscience*, *4*, Article 18. https://doi.org/10.1186/s43170-023-00145-7
13. Chang, W., Yang, S., Xi, X., Wang, H., Liu, Z., Zhang, X., & Li, S. (2025). Classification of seed maize using deep learning and transfer learning based on time series spectral feature reconstruction of remote sensing. *Computers and Electronics in Agriculture*, *236*, 110256. https://doi.org/10.1016/j.compag.2025.110256
14. Eisfelder, C., Boemke, B., Gessner, U., Sogno, P., Alemu, G., Hailu, R., … Huth, J. (2024). Cropland and crop type classification with Sentinel-1 and Sentinel-2 time series using Google Earth Engine for agricultural monitoring in Ethiopia. *Remote Sensing*, *16*(5), 866. https://doi.org/10.3390/rs16050866
15. Gitas, I. Z., Mitri, G. H., & Al-Hourani, A. (2019). Multi-seasonal WorldView-3 imagery for discriminating olive and fig trees. *International Journal of Remote Sensing*, *40*(15), 5890–5905. https://doi.org/10.1080/01431161.2019.1580821
16. Heiss, N., Meier, J., Gessner, U., & Kuenzer, C. (2025). A review: Potential of Earth Observation (EO) for mapping small-scale agriculture and cropping systems in West Africa. *Land*, *14*(1), 171. https://doi.org/10.3390/land14010171
17. Hill, J., Schulz, C., & Müller, A. (2018). Using multi-temporal Sentinel-2 satellite images to distinguish apple and pear orchards in Germany. *Remote Sensing of Environment*, *215*, 145–153.

https://doi.org/10.1016/j.rse.2018.06.012

18. Huang, J., Xiao, G., Li, X., Zheng, J., Zeng, Y., & Su, W. (2026). Progress and perspectives of crop type mapping with remote sensing: A review. *IEEE Geoscience and Remote Sensing Magazine*, *14*(3), 129–162. https://doi.org/10.1109/MGRS.2025.3648119
19. Jin, Z., Azzari, G., You, C., Di Tommaso, S., Aston, S., Burke, M., & Lobell, D. B. (2019). Smallholder area and yield mapping at national scales with Google Earth Engine. *Remote Sensing of Environment*, *228*, 115–128. https://doi.org/10.1016/j.rse.2019.04.016
20. Khalili-Moghadam, A., & Saeidi, Z. (2023). Ant fauna of walnut orchards of the Shahrekord and Saman Counties (Chaharmahal & Bakhtiari Province) with the report of some ant species as symbiont of walnut aphids. *Journal of the Entomological Society of Iran*, *43*(1), 23–34. https://doi.org/10.22117/jesi.2023.358116.1507
21. Kussul, N., Lavreniuk, M., Skakun, S., & Shelestov, A. (2017). Deep learning classification of land cover and crop types using remote sensing data. *IEEE Geoscience and Remote Sensing Letters*, *14*(5), 778–782. https://doi.org/10.1109/LGRS.2017.2681128
22. Liakos, K. G., Busato, P., Moshou, D., Pearson, S., & Bochtis, D. (2018). Machine learning in agriculture: A review. *Sensors*, *18*(8), 2674. https://doi.org/10.3390/s18082674
23. Liu, Y., Xu, W., & Chen, H. (2024). Topographic controls on rice suitability in the lower Mekong Basin: A combined slope aspect wetness approach. *Agricultural Water Management*, *295*, 108765. https://doi.org/10.1016/j.agwat.2024.108765
24. Low, F., & Duveiller, G. (2015). Defining the optimal temporal resolution for crop type mapping based on remote sensing data. *Remote Sensing*, *7*(10), 12791–12813. https://doi.org/10.3390/rs71012791
25. Machireddy, S. R. (2023). Mapping and change detection analysis of land use / land cover by using geospatial technologies. *International Journal of Creative Research Thoughts (IJCRT)*, *11*(8), c758–c765. http://www.ijcrt.org/papers/IJCRT2308297.pdf
26. Mirzaei, S., Vafakhah, M., Pradhan, B., & Alavi, S. J. (2020). An improved land use classification scheme using multi-seasonal satellite images and secondary data. *ECOPERSIA*, *8*(2), 97–107.
27. Mishra, B., & Susaki, J. (2014). Optical and SAR data integration for automatic change pattern detection. *ISPRS Annals of Photogrammetry, Remote Sensing and Spatial Information Sciences*, *II-7*, 39–46. https://doi.org/10.5194/isprsannals-II-7-39-2014
28. Mobarakeh, Z. M., Pourmanafi, S., & Ahmadi, M. (2025). Employing Sentinel-2 time-series and noisy data quality control enhance crop classification in arid environments: A comparison of machine learning and deep learning methods. *International Journal of Applied Earth Observation and Geoinformation*, *142*, 104678. https://doi.org/10.1016/j.jag.2025.104678
29. Narimani, M., Pourreza, A., Moghimi, A., & Farajpoor, P. (2026). Sentinel-2 for crop yield estimation: A systematic review. *arXiv preprint, arXiv:2603.23779*. https://doi.org/10.48550/arXiv.2603.23779
30. Pena, J. M., Gutiérrez, P. A., Hervás-Martínez, C., & López-Granados, F. (2017). Object-based image classification of summer crops with machine learning methods. *Remote Sensing*, *9*(10), 1033. https://doi.org/10.3390/rs9101033

31. Peng, W., Ye, H., Qiao, S., Liu, R., Nie, C., Zhang, B., … Huang, S. (2023). Early crop mapping based on Sentinel-2 time-series data and the Random Forest algorithm. *Remote Sensing*, *15*(13), 3212. https://doi.org/10.3390/rs15133212
32. Qi, H., Qian, X., Shang, S., & Wan, H. (2024). Multi-year mapping of cropping systems in regions with smallholder farms from Sentinel-2 images in Google Earth Engine. *GIScience & Remote Sensing*, *61*(1), Article 2309843. https://doi.org/10.1080/15481603.2024.2309843
33. Rehman, A. U., Shrestha, B., & Zhang, L. (2025). A deep learning based novel spectral matching technique for orchards classification using spectrotemporal signatures leveraging multidimensional data format. *International Journal of Digital Earth*, *18*(1), 2548381. https://doi.org/10.1080/17538947.2025.2548381
34. Swain, P. H., & Davis, S. M. (1978). *Remote Sensing: The Quantitative Approach*. McGraw-Hill.
35. Wang, M., Liu, X., Zhang, X., & Liu, W. (2021). A review of random forest in remote sensing for crop mapping. *Remote Sensing Letters*, *12*(8), 789–798. https://doi.org/10.1080/2150704X.2021.1931526
36. Zhan, C., Liu, B., & Li, Z. (2022). Rice paddy mapping in tropical floodplains using multi-temporal Sentinel-1 and topographic indices. *Remote Sensing of Environment*, *278*, 113079. https://doi.org/10.1016/j.rse.2022.113079
37. Zhang, L., Liu, X., & Wang, Y. (2025). A new approach for spatial-temporal monitoring of subtropical forest types using Google Earth Engine and machine learning algorithms. *Remote Sensing*, *17*(8), 1356. https://doi.org/10.3390/rs17081356
38. Zhou, X.-X., Li, Y.-Y., Luo, Y.-K., Sun, Y.-W., Su, Y.-J., Tan, C.-W., & Liu, Y.-J. (2022). Research on remote sensing classification of fruit trees based on Sentinel-2 multi-temporal imageries. *Scientific Reports*, *12*(1), 11549. https://doi.org/10.1038/s41598-022-15414-0

Figures

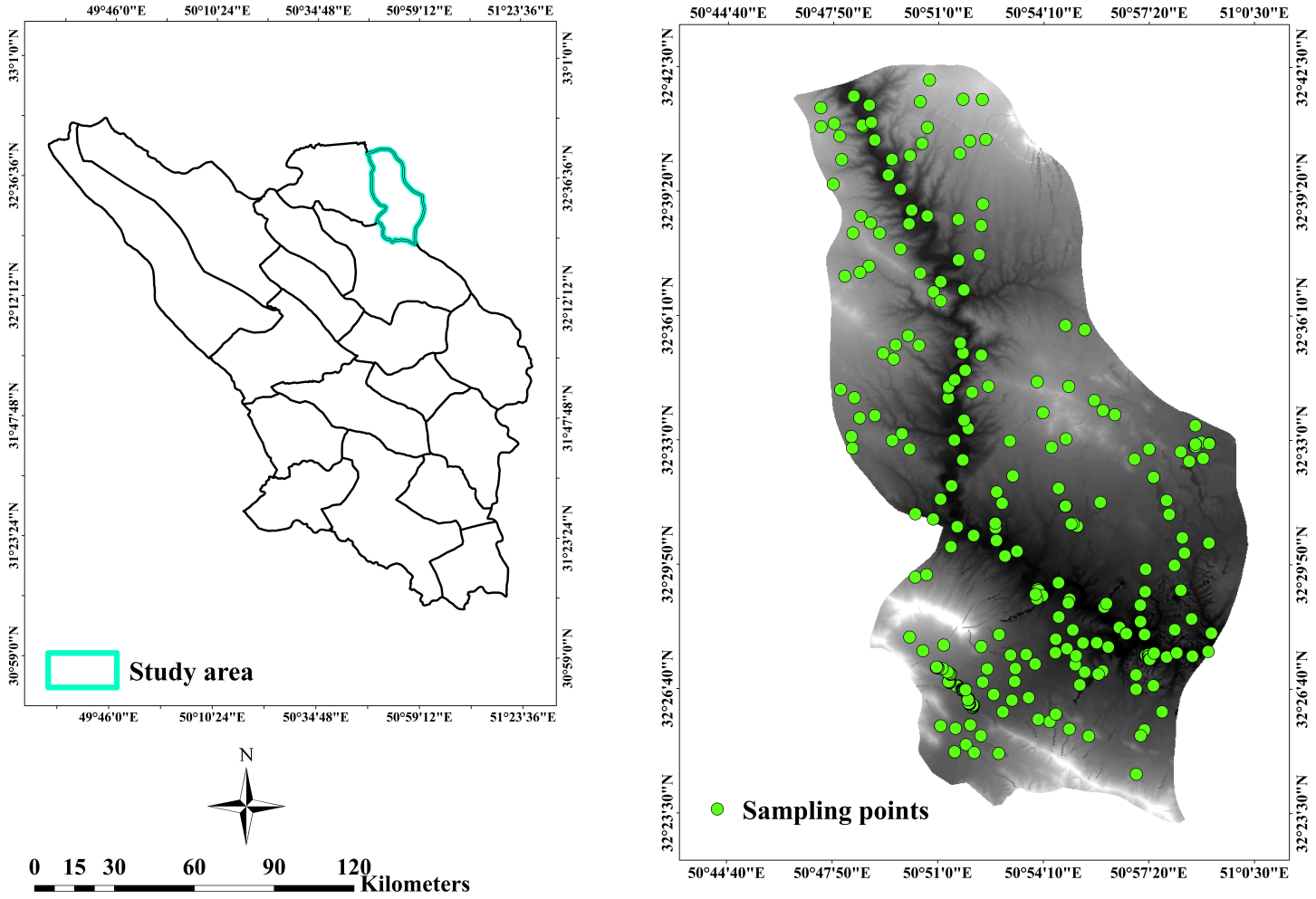


Figure 1

Location of the study area: (a) Chaharmahal-Va-Bakhtiari province boundary; (b) study area boundary (Saman district). A set of sampling points was collected from agricultural areas. The sampling points were subsequently divided into two groups: 70% for training the crop-type classification model and 30% for testing and validation mapping.

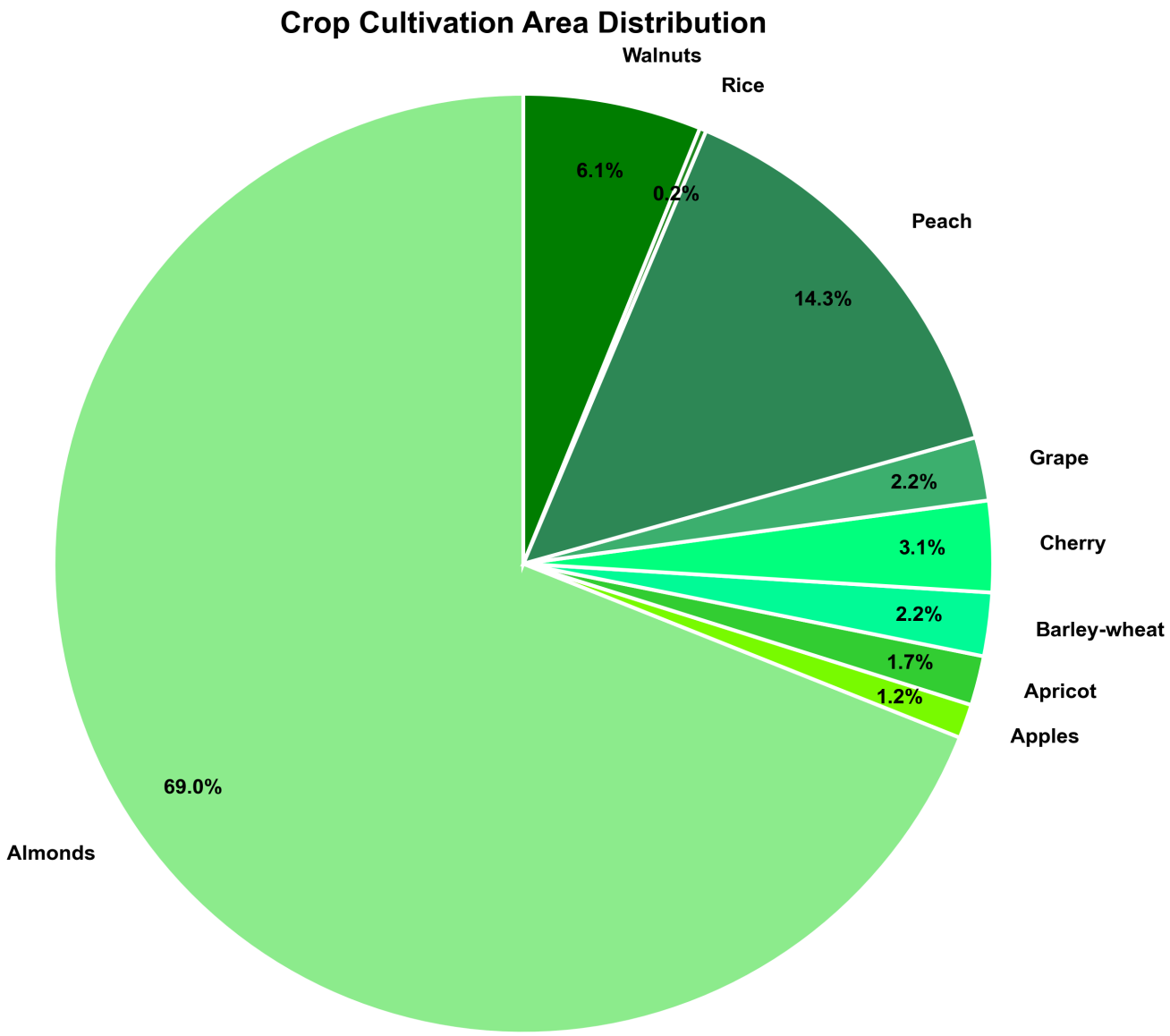


Figure 2

Percentage of cultivated area for selected agricultural crop types, based on the Agricultural Yearbook.

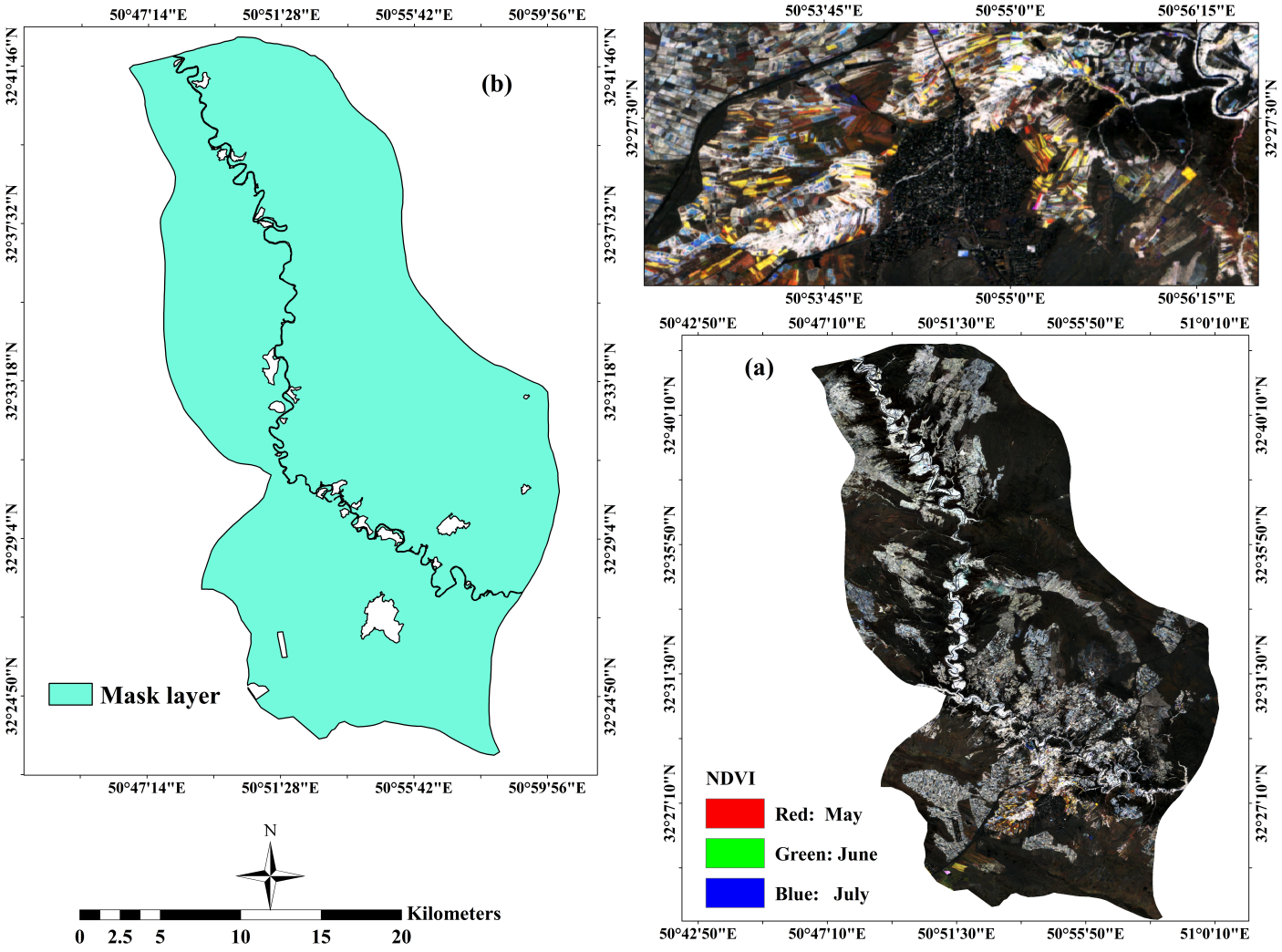


Figure 3

Separation of residential areas and generation of the mask layer. (a) False-color composite of NDVI; (b) Mask layer produced by excluding residential areas.

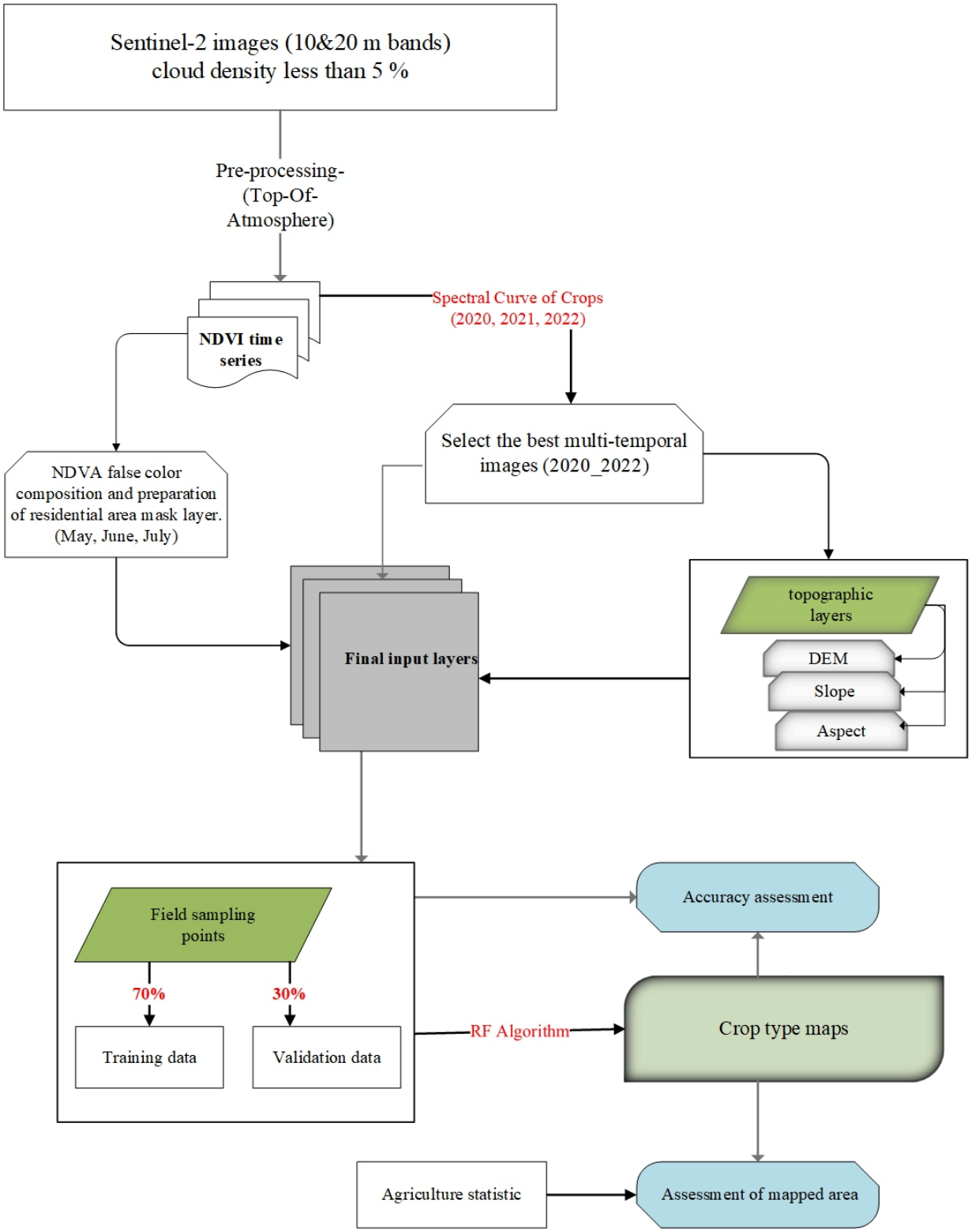


Figure 4

Methodological workflow for crop type mapping: (1) Sentinel-2 image acquisition and preprocessing; (2) NDVI time-series analysis and optimal temporal window selection via TD; (3) Residential area masking using NDVI false-color composites; (4) Incorporation of topographic layers; (5) RF classification on GEE; (6) Accuracy assessment using independent validation points; (7) Comparison with agricultural statistics.

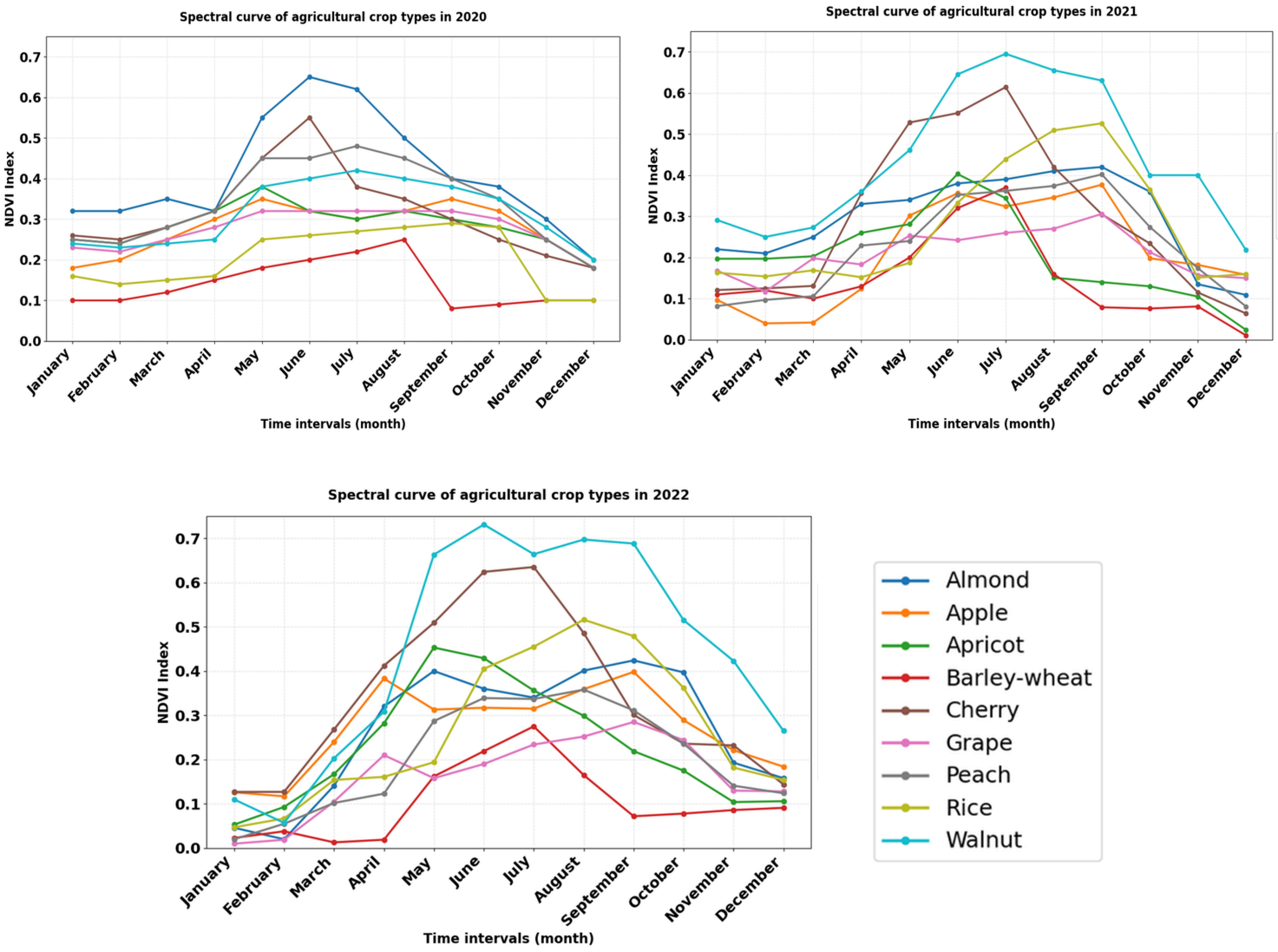


Figure 5

Spectral-temporal curves of the NDVI for 9 agricultural crop types in the years 2020–2022.

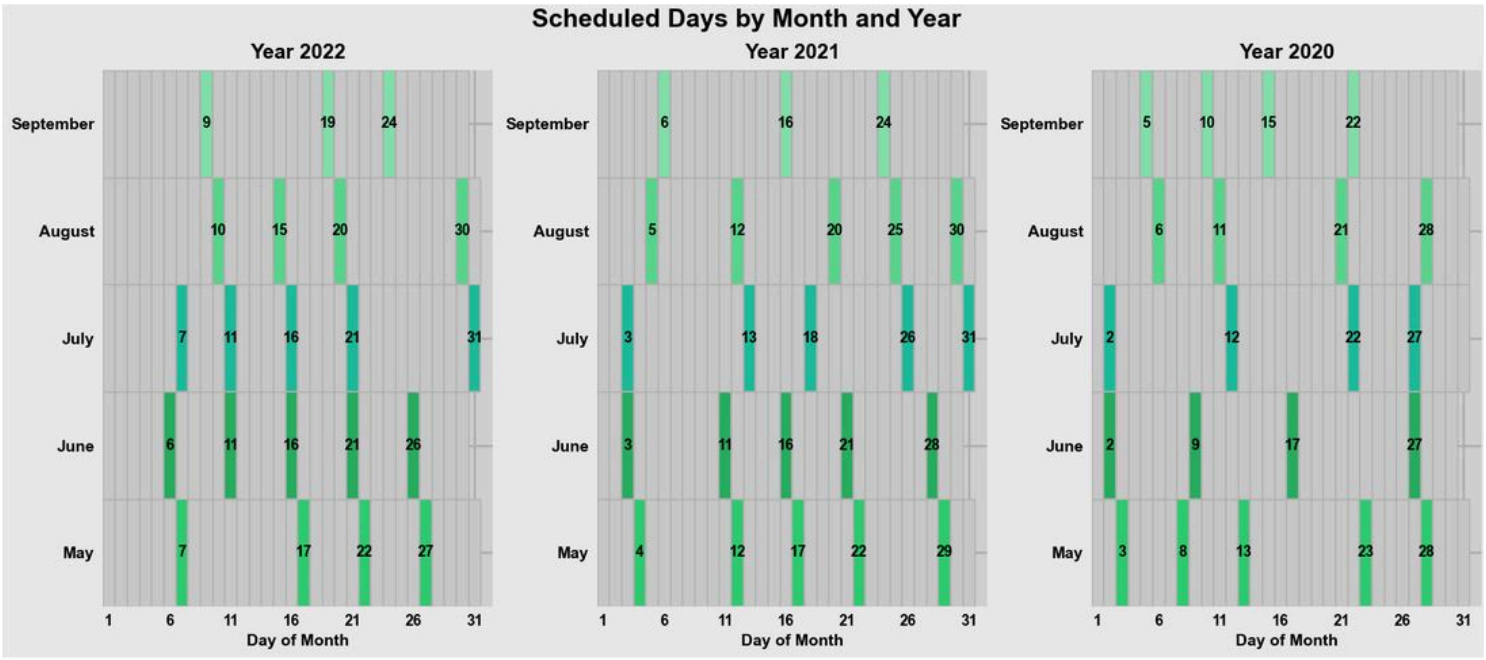


Figure 6

Best-performing Sentinel-2 temporal composites for crop type mapping.

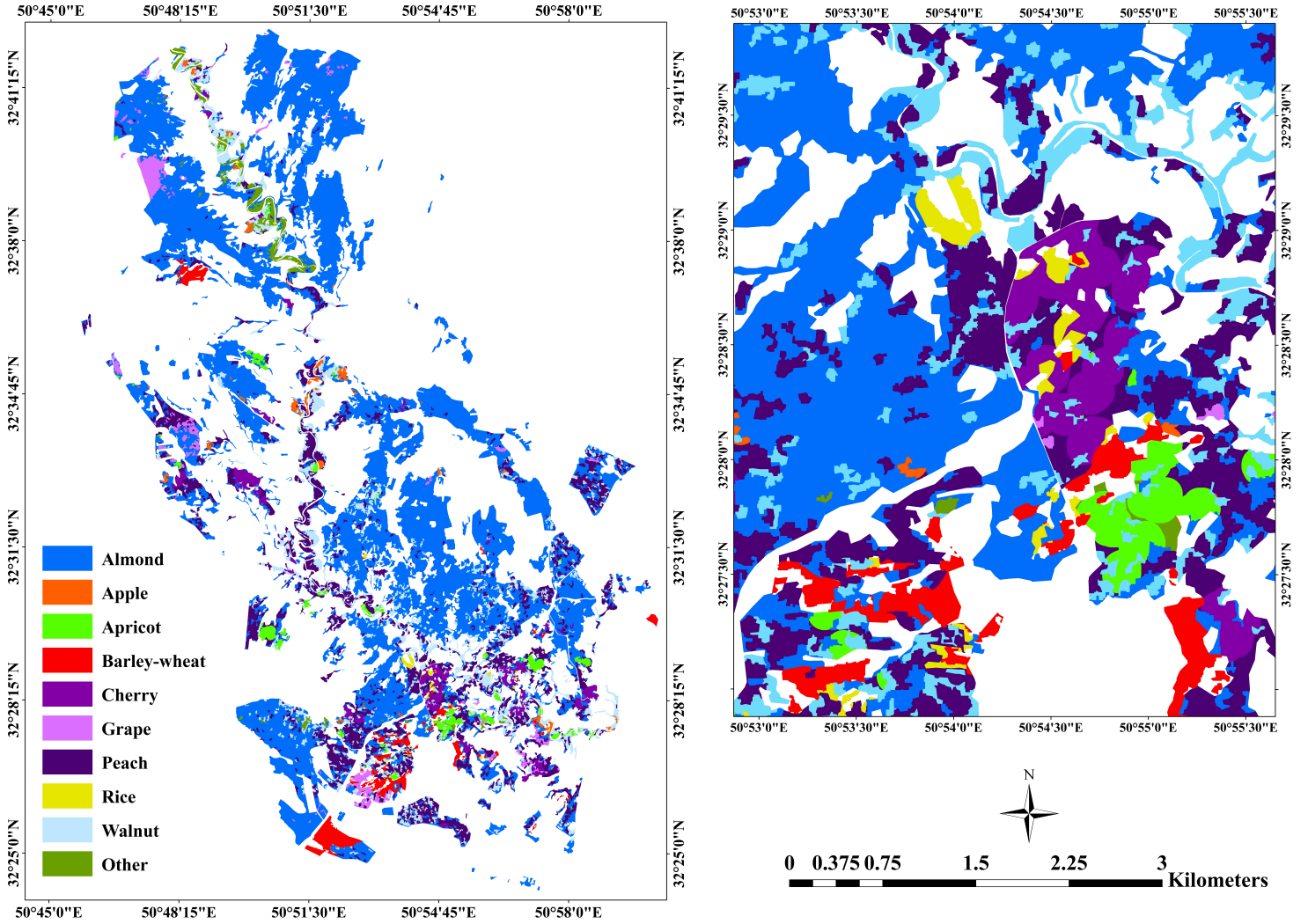


Figure 7

Crop type classification mapping.

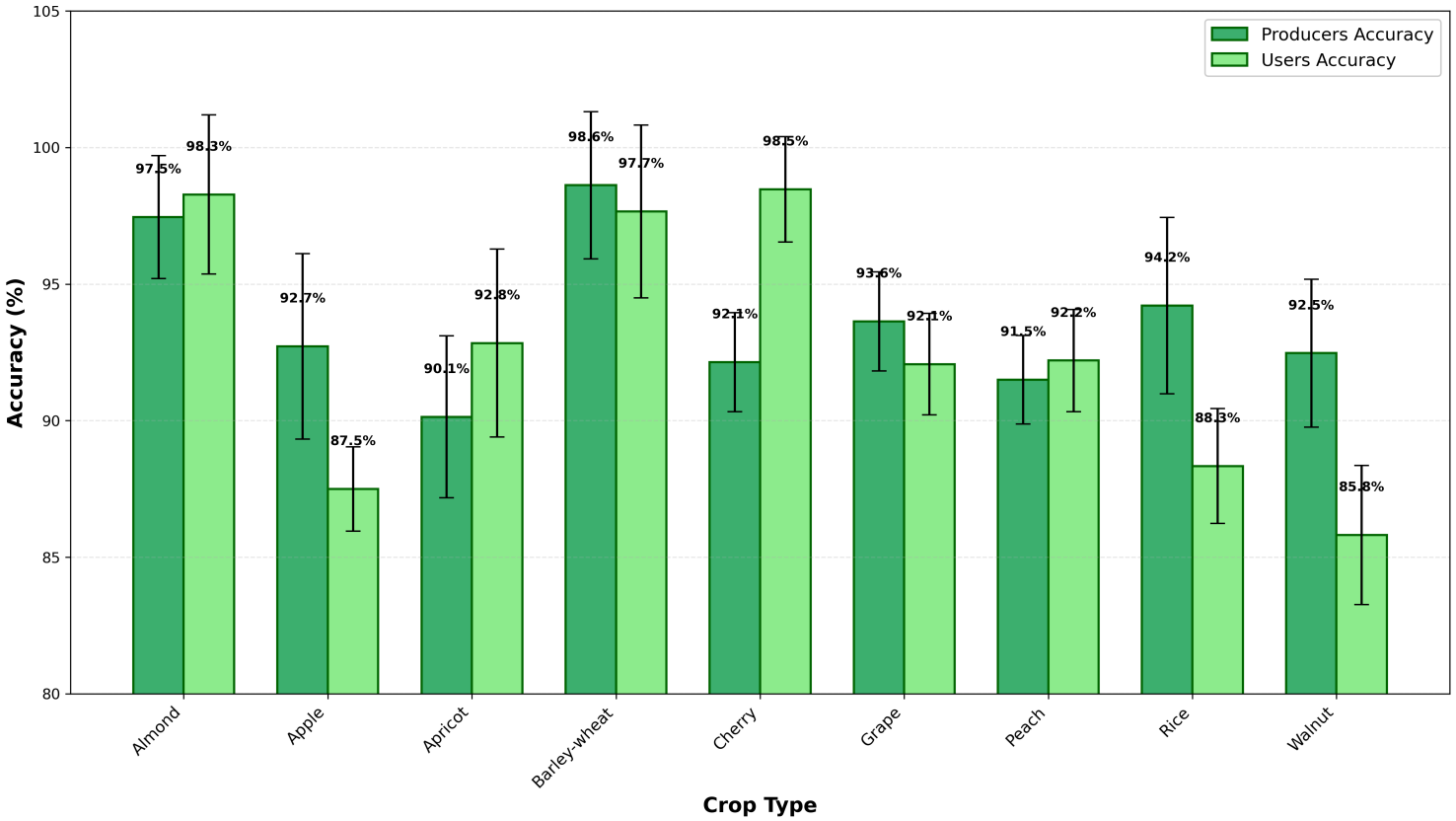


Figure 8

Comparison of Producer's Accuracy and User's Accuracy by Crop Type

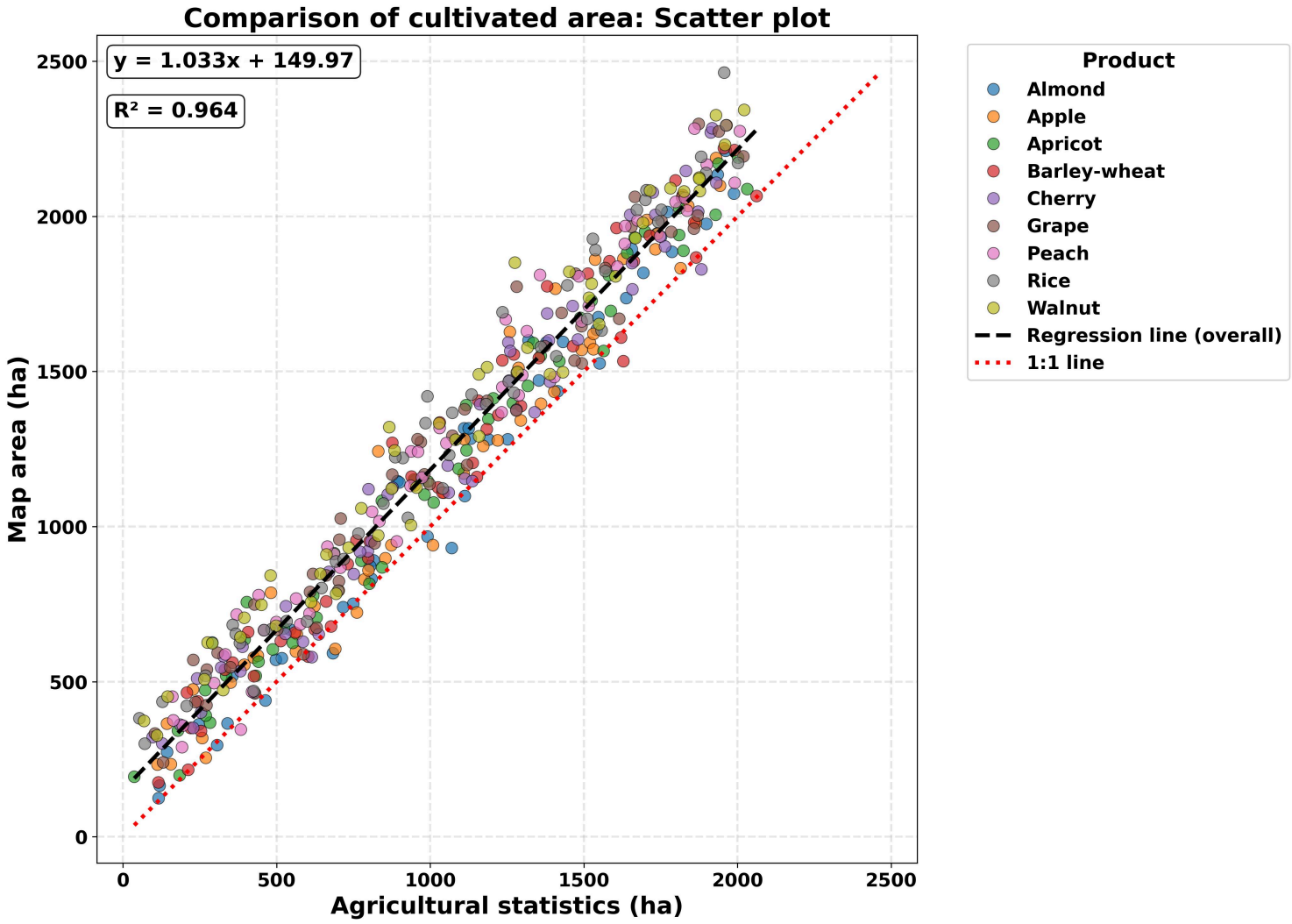


Figure 9

Scatter Plot comparing the cultivated area from statistical yearbooks and the crop type classified map.

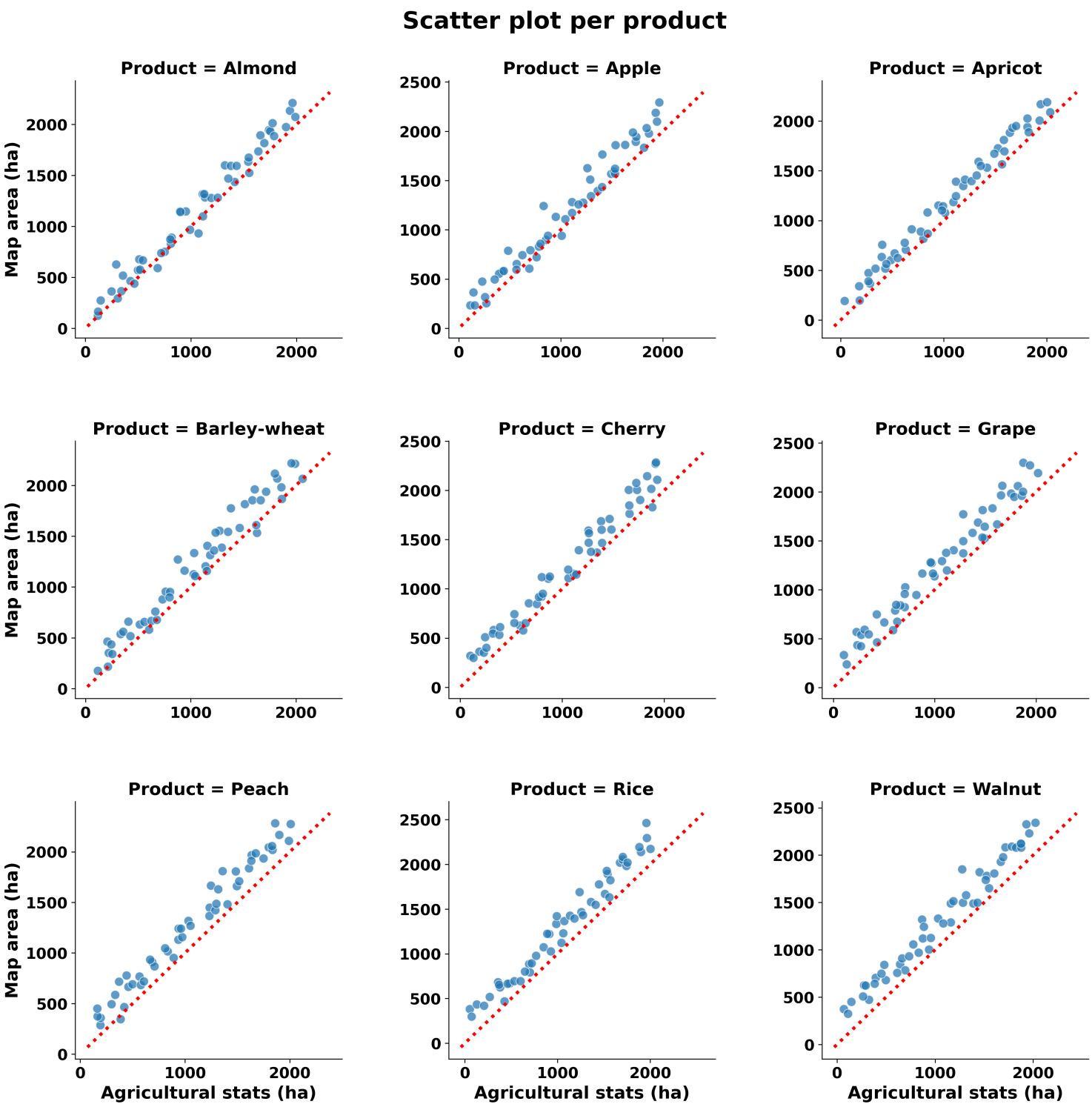


Figure 10

Per-class scatter plots comparing map-derived cultivated areas with official agricultural statistics for each crop type.